J. Fluid Mech. (1997), *vol.* 335, *pp.* 141–163

Effects of weak wind and damping on Wilton's ripples

By KARSTEN TRULSEN[1] AND CHIANG C. MEI[2]

[1]Department of Mathematics, University of Bergen, Johannes Brunsgate 12, N–5008 Bergen, Norway

[2]Department of Civil and Environmental Engineering, Massachusetts Institute of Technology, Cambridge, MA 02139, USA

(Received 20 May 1996 and in revised form 13 September 1996)

A model for second-harmonic resonance between two gravity–capillary waves is derived, for the case where weak wind and laminar viscosity are of comparable importance. It is revealed that there exist two threshold wind speeds. For winds weaker than the lower threshold, waves are damped. For winds stronger than the upper threshold, the wave energy becomes unbounded and the spectrum cannot be confined to two resonating harmonics. In the intermediate range there exist steady progressive combination waves of the first and second harmonics. These are Wilton's ripples in equilibrium with wind input and viscous dissipation, and are probably physically observable.

1. Introduction

Theoretical study of resonant interactions between gravity–capillary waves was initiated by Harrison (1909) and Wilton (1915). Wilton (1915) solved the steady progressive waves resulting from exact second-harmonic resonance. Wilton's solution was generalized to allow for detuning by Pierson & Fife (1961). These waves are now known as steady Wilton's ripples. McGoldrick (1965) and Simmons (1969) later derived evolution equations for general triad resonance. Indeed, McGoldrick (1970) pointed out that the steady solutions of Wilton (1915) correspond to special initial conditions for the general triad resonance theory. Nayfeh (1973) considered inviscid conservative Wilton's ripples in the presence of a uniform air flow above the water surface.

Jones (1992) derived cubic nonlinear evolution equations for Wilton's ripples to investigate their slow time and space modulation. A nonlinear stability analysis was presented for uniform wave solutions. Christodoulides & Dias (1994) considered nonlinear steady Wilton's ripples on the interface between two fluids of different densities. They let each wave consist of two components propagating in opposite directions, and found them to be coupled at the third order. They also found that new bifurcations arise when the density ratio is varied.

Bifurcations of steady wave trains subject to harmonic resonance were studied by Chen & Saffman (1979). They showed that steady Wilton's ripples are associated with a period-doubling bifurcation, through which a pure second-harmonic wave can become a combination wave of the first and second harmonics.

Motivated by nonlinear wave interactions under strong wind, Morland (1994)

studied the modification of the resonance condition due to drift current, but excluded the direct effect of wind. He assumed the current to be as strong as the phase velocity and solved the linearized Rayleigh equation for the disturbance in water.

All these theories are based on the assumption of an inviscid fluid without dissipation or wind forcing. Because of viscosity, gravity–capillary waves cannot be sustained unless there is an external energy supply. Theories on the conservative long-time nonlinear evolution of these waves are therefore not readily applicable to many phenomena observed either in nature or in the laboratory.

To explain the frequency downshift of short waves observed in a wind tunnel by Choi (1977) and Ramamonjiarisoa, Baldy & Choi (1978), Janssen (1986) investigated the initial growth of Wilton's ripples subject to wind forcing and viscous damping. He found that the wind can give rise to period doubling of the waves, i.e. from the second to the first harmonic of a Wilton's ripple. Janssen (1987) later applied the theory of Zakharov and generalized to a continuous spectrum of waves subject to three-dimensional resonant triad interaction with wind forcing. He found that under certain conditions there may be a sudden migration of the peak of the spectrum to lower wavenumbers. In both papers Janssen (1986, 1987) employed a wind forcing that is much stronger than the damping due to viscosity, and hence the theory is only valid for a limited time before the wave amplitudes become too large. Bontozoglou & Hanratty (1990) explained the observation of Choi (1977) by a Kelvin–Helmholtz instability mechanism. However, their theory is for strong winds and highly viscous fluids, and therefore more relevant to engineering than to geophysical applications. Jurman, Deutsch & McCready (1992) presented theory and experiment on centimetre-range wind-driven surface waves on a highly viscous fluid (viscosity 10–100 times greater than water). After adjusting the gas flow to be just sufficient to produce measurable waves, they observed that the wave of highest linear growth rate due to wind could saturate at a small steepness, while energy was transferred to its second harmonic which was linearly damped.

Among existing theories on non-conservative triad interaction, one class deals with the case where the highest-frequency wave is subject to external forcing while the lowest-frequency wave is damped. Consistent with the so-called decay instability of waves, energy is transferred to the lowest-frequency wave by nonlinearity and then dissipated. The resulting behaviour often leads to chaos through a series of period-doubling bifurcations of the wave envelope. This behaviour has been reported for applications in plasma physics (e.g. Vyshkind & Rabinovich 1976; Wersinger, Finn & Ott 1980*a, b*). In a second class, the highest-frequency wave is damped while the lowest-frequency wave is subject to external forcing, and energy is transferred to the highest-frequency wave by nonlinearity and then dissipated. In such cases one often does not find chaotic behaviour, but the energy may blow up after a finite time unless the forcing is weak. This has been reported for applications in hydrodynamics (e.g. McDougall & Craik 1991; Hughes & Proctor 1992). Analytical solutions for certain special cases of non-conservative triad interaction were given by Miles (1976) and Craik (1986). Chow, Bers & Ram (1992) showed that non-conservative space–time evolution of the equations for triad resonance may yield spatio–temporal chaos; their work belongs to the first class.

The effects of wind and viscosity on the nonlinear evolution of narrow-banded gravity–capillary waves has been investigated theoretically by Hara & Mei (1994).

In this paper we shall examine the effects of weak wind and damping on Wilton's ripples. Specifically, the wind forcing and viscous damping are of smaller magnitude than the quadratic interactions that are responsible for triad resonance (cf. the

discussion on viscous damping in Trulsen & Mei 1995). While the inviscid theory tells us that nonlinearity and dispersion can achieve dynamical balance to yield certain permanent wave envelopes (Wilton 1915), we wish to examine how this balance may be altered by slightly non-conservative effects. The general behaviour is found to belong to the second class mentioned above.

After first summarizing the basic governing equations in §2 and the basic wind profile in §3, scaling assumptions are described in §4 to facilitate a multiple-scales perturbation analysis. The approximate equations are summarized in §5. Then the perturbation analysis is carried out for the wave disturbance in water in §6 and in air in §7. The resulting dynamical system for time evolution is summarized at the end of §6. At the leading (second) order the dynamical system is Hamiltonian, and its complete solution is presented in §8. The behaviour of the full non-conservative system at the third order is discussed in §9.

2. Governing equations

Let x and z denote the horizontal and vertical coordinates, and $\nabla = (\partial/\partial x, \partial/\partial z)$ denote the gradient operator. The steady part of the fluid flow has a horizontal velocity $\boldsymbol{U}^S = (U^S(z), 0)$. The part due to wave disturbance has velocity $\boldsymbol{u} = (u, w)$, pressure p, and surface displacement η. The density is denoted by ρ, the kinematic viscosity by ν, and the surface tension between water and air by Γ. Quantities in water are unprimed, while corresponding quantities in air are distinguished by primes.

The continuity and momentum conservation equations for the wave disturbance in water are as follows, with similar equations in air for the primed quantities:

$$\nabla \cdot \boldsymbol{u} = 0, \tag{2.1}$$

and

$$\frac{\partial \boldsymbol{u}}{\partial t} + \boldsymbol{u} \cdot \nabla \boldsymbol{u} + \boldsymbol{u} \cdot \nabla \boldsymbol{U}^S + \boldsymbol{U}^S \cdot \nabla \boldsymbol{u} = -\frac{1}{\rho} \nabla p + \nu \nabla^2 \boldsymbol{u}. \tag{2.2}$$

At the water surface, the velocity is continuous,

$$\boldsymbol{u} + \boldsymbol{U}^S = \boldsymbol{u}' + \boldsymbol{U}'^S \qquad \text{at} \quad z = \eta. \tag{2.3}$$

The kinematic surface condition is

$$\frac{\partial \eta}{\partial t} + (u + U^S) \frac{\partial \eta}{\partial x} = w \qquad \text{at} \quad z = \eta. \tag{2.4}$$

Let the unit normal and tangential vectors to the sea surface be denoted by $\boldsymbol{n}$ and $\boldsymbol{t}$, respectively. Continuity of the normal stress requires that

$$-\frac{p}{\rho} + g\eta + 2\nu \boldsymbol{n} \cdot \nabla (\boldsymbol{u} + \boldsymbol{U}^S) \cdot \boldsymbol{n} + \frac{\Gamma}{\rho} \nabla \cdot \boldsymbol{n} = N \qquad \text{at} \quad z = \eta, \tag{2.5}$$

where N is proportional to the normal stress exerted by air

$$N = \frac{\rho'}{\rho} \left\{ -\frac{p'}{\rho'} + g\eta + 2\nu' \boldsymbol{n} \cdot \nabla (\boldsymbol{u}' + \boldsymbol{U}'^S) \cdot \boldsymbol{n} \right\} \qquad \text{at} \quad z = \eta. \tag{2.6}$$

Continuity of the tangential stress requires that

$$\boldsymbol{t} \cdot \nabla (\boldsymbol{u} + \boldsymbol{U}^S) \cdot \boldsymbol{n} + \boldsymbol{n} \cdot \nabla (\boldsymbol{u} + \boldsymbol{U}^S) \cdot \boldsymbol{t} = T \qquad \text{at} \quad z = \eta, \tag{2.7}$$

where T is proportional to the tangential stress exerted by air,

$$T = \frac{\rho' \nu'}{\rho \nu} \left\{ \boldsymbol{t} \cdot \nabla (\boldsymbol{u}' + \boldsymbol{U}'^S) \cdot \boldsymbol{n} + \boldsymbol{n} \cdot \nabla (\boldsymbol{u}' + \boldsymbol{U}'^S) \cdot \boldsymbol{t} \right\} \qquad \text{at} \quad z = \eta. \tag{2.8}$$

We also require that the wave disturbance dies out at large depth and height.

The pressure can be eliminated from (2.5)–(2.6) by taking the directional derivative along the surface, $\boldsymbol{t} \cdot \nabla$, and then substituting $\boldsymbol{t} \cdot \nabla p$ from the momentum equation:

$$\boldsymbol{t} \cdot \left\{ \frac{\partial \boldsymbol{u}}{\partial t} + \boldsymbol{u} \cdot \nabla \boldsymbol{u} + \boldsymbol{u} \cdot \nabla \boldsymbol{U}^S + \boldsymbol{U}^S \cdot \nabla \boldsymbol{u} - \nu \nabla^2 \boldsymbol{u} \right.$$
$$\left. + \nabla \left(g\eta + 2\nu \boldsymbol{n} \cdot \nabla (\boldsymbol{u} + \boldsymbol{U}^S) \cdot \boldsymbol{n} + \frac{\Gamma}{\rho} \nabla \cdot \boldsymbol{n} \right) \right\} = \boldsymbol{t} \cdot \nabla N \qquad \text{at} \quad z = \eta, \tag{2.9}$$

where the pressure can be eliminated from N similarly.

Let us introduce the stream functions

$$\boldsymbol{u} = \left(\frac{\partial \psi_w}{\partial z}, -\frac{\partial \psi_w}{\partial x} \right), \qquad U^S = \frac{\partial \Psi^S}{\partial z}, \tag{2.10}$$

with similar definitions of primed quantities in the air. The pressure can be eliminated from the momentum equation by taking the curl, and the resulting governing equation for the stream function ψ_w becomes

$$\frac{\partial}{\partial t} \nabla^2 \psi_w - \frac{\partial (\psi_w + \Psi^S, \nabla^2 (\psi_w + \Psi^S))}{\partial (x, z)} - \nu \nabla^4 \psi_w = 0. \tag{2.11}$$

Similarly, the stream functions can be substituted into the surface conditions in a straightforward manner.

3. Steady wind and wind-induced drift

The friction velocities in air and water, u'_* and u_*, are related to the shear stress on the undisturbed water surface τ^S through the relationships $u_* = (\tau^S/\rho)^{1/2}$ and $u'_* = (\tau^S/\rho')^{1/2}$.

The usual linear–logarithmic shear profile will be employed for the wind and the induced current (cf. Miles 1962; Valenzuela 1976; Kawai 1979; Gastel, Janssen & Komen 1985; Hara & Mei 1994). Thus the wind profile is

$$U'^S = \begin{cases} U_d + \dfrac{u'^2_*}{\nu'} z, & z \leqslant 5 \dfrac{\nu'}{u'_*} \\ U_d + 5u'_* + \dfrac{u'_*}{\kappa} (\alpha - \tanh \tfrac{1}{2}\alpha), & z > 5 \dfrac{\nu'}{u'_*}, \end{cases} \tag{3.1}$$

where

$$\sinh \alpha = 2\kappa \frac{u'_*}{\nu'} \left(z - 5 \frac{\nu'}{u'_*} \right), \tag{3.2}$$

and where U_d is the drift velocity of the water surface and $\kappa = 0.4$ is the universal Kármán constant. The viscous sublayer height of the wind profile is $5\nu'/u'_*$.

In water the drift current is

$$U^S = \begin{cases} U_d + \dfrac{u^2_*}{\nu} z, & z \geqslant -5 \dfrac{\nu}{u_*} \\ U_d - 5u_* + \dfrac{u_*}{\kappa} (\alpha - \tanh \tfrac{1}{2}\alpha) & z < -5 \dfrac{\nu}{u_*}, \end{cases} \tag{3.3}$$

where

$$\sinh\alpha = 2\kappa\frac{u_*}{\nu}\left(z + 5\frac{\nu}{u_*}\right). \tag{3.4}$$

The viscous sublayer depth of the current profile is $5\nu/u_*$.

The wind model requires knowledge of the relationship between the drift velocity U_d and the friction velocity in air u'_*. Our attention will be restricted to wind strengths corresponding to an air friction velocity of less than approximately 0.17 m s^{-1}. In this range, existing experimental data (Gastel *et al.* 1985) suggest the empirical relation $U_d = 0.565\,u'_*$ which we shall employ here.

4. Scaling assumptions

Denoting the wavenumber and the frequency of the first harmonic of Wilton's ripples by

$$\bar{k} = \left(\frac{\rho g}{2\Gamma}\right)^{1/2} \qquad \text{and} \qquad \bar{\omega} = \left(\frac{3g\bar{k}}{2}\right)^{1/2}, \tag{4.1}$$

we shall use their reciprocals to normalize (x, z) and t respectively. The order of magnitude of the inviscid wave disturbance in water and air is clearly

$$\eta \sim a, \qquad \psi_w, \psi'_w \sim \frac{\bar{\omega}a}{\bar{k}}, \tag{4.2}$$

where a is a typical wave amplitude. Assuming gentle wave steepness, we shall use the small parameter

$$\epsilon = \bar{k}a \ll 1 \tag{4.3}$$

as the principal measure to characterize small quantities in our discussion.

It is well known that in the absence of wind and damping, nonlinear interactions of Wilton's ripples occur at the second order, $O(\epsilon^2)$, while the time scale for nonlinear development is $\bar{\omega}t = O(1/\epsilon)$. In order to examine the modification by and competition between viscous damping and wind forcing, we shall introduce several order-of-magnitude assumptions such that the two physical effects will be of comparable importance at the third order in wave steepness. First we assume that the steady wind velocity is comparable to the phase velocity of the waves, while the wind-induced current in water is much smaller. Accordingly, the following normalizations are introduced:

$$\left.\begin{gathered} \bar{k}(x,z) \to (x,z), \qquad \bar{\omega}t \to t, \\ \bar{k}\eta \to \epsilon\eta, \qquad \bar{k}^2\bar{\omega}^{-1}(\psi_w, \psi'_w) \to (\epsilon\psi_w, \epsilon\psi'_w), \\ \bar{k}\bar{\omega}^{-1}(U^S, U_d, U'^S) \to (\epsilon U^S, \epsilon U_d, U'^S). \end{gathered}\right\} \tag{4.4}$$

Next we let the ratio between the densities be second order in ϵ:

$$\frac{\rho'}{\rho} \sim \epsilon^2. \tag{4.5}$$

Consistent with the typical kinematic viscosities in water and air, we estimate that

$$\frac{\nu\bar{k}^2}{\bar{\omega}} \sim \epsilon^2, \qquad \frac{\nu'\bar{k}^2}{\bar{\omega}} \sim \epsilon. \tag{4.6a,b}$$

Thus the dimensionless viscous damping in water is of the order ϵ^2, one order smaller than that of nonlinearity. Our assumptions also ensure that the ratios U^S/U'^S and

ν/ν' are both of order $(\rho'/\rho)^{1/2} \sim \epsilon$, consistent with the continuity of turbulent shear stress across the sea surface.

There can be three wave-induced viscous boundary layers. In the surface boundary layer in water the linear terms dominate the balance of horizontal momentum, while the tangential stress on the surface is small, leading to the dominant balance in physical variables

$$\frac{\partial u}{\partial t} - \nu \frac{\partial^2 u}{\partial z^2} \approx 0 \qquad \text{with} \qquad \frac{\partial u}{\partial z} \approx 0 \quad \text{at} \quad z = \eta. \tag{4.7}$$

Hence the dimensionless thickness is $O(\epsilon)$ in view of (4.6*a*). The appropriate vertical boundary-layer coordinate and decomposition of the stream function into inviscid and boundary-layer components are

$$z_{BL} = \epsilon^{-1} z, \qquad \psi_w = \psi + \epsilon^2 \psi_{BL}. \tag{4.8}$$

In air there is also a surface boundary layer. For a weak wind, the linear terms dominate the balance of horizontal momentum, while there is little slip on the surface, i.e.

$$\frac{\partial u'}{\partial t} - \nu' \frac{\partial^2 u'}{\partial z^2} \approx 0 \qquad \text{with} \qquad u' = u \quad \text{at} \quad z = \eta. \tag{4.9}$$

Hence this boundary-layer has dimensionless thickness $O(\epsilon^{1/2})$ in view of (4.6*b*).

Above the sea surface, there is an internal layer at the critical height where the wind speed is equal to the phase velocity of the wave, implying

$$\frac{\partial u'}{\partial t} + U'^S \frac{\partial u'}{\partial x} \approx 0. \tag{4.10}$$

In this internal layer the dominant balance of the horizontal momentum is expressed by

$$\frac{\partial U'^S}{\partial z} w' - \nu' \frac{\partial^2 u'}{\partial z^2} \approx 0. \tag{4.11}$$

Hence the dimensionless thickness of the internal layer is $O(\epsilon^{1/3})$.

For a vanishingly weak wind such that the waves are damped, the two viscous shear layers in air are well separated from each other. For a strong wind such that the waves grow steadily, these layers coalesce (e.g. Gastel *et al.* 1985). For moderately weak winds, the two layers can overlap partially, rendering the physics complicated and analytical treatment ineffective. Hence we shall solve the wave disturbance in air numerically without separating the viscous and inviscid parts. An estimate of the importance of the viscous shear layers in air can be discerned by letting

$$z'_{BL} = \mu^{-1} z, \qquad \psi'_w = \psi' + \mu \psi'_{BL} \qquad \text{with} \qquad \epsilon^{1/2} \leqslant \mu \leqslant \epsilon^{1/3}. \tag{4.12}$$

As a quantitative check of these scaling assumptions, we take the following values for surface tension, gravitational acceleration, densities and laminar viscosities at 20°C:

$$\Gamma = 7.28 \times 10^{-2}\ \text{N m}^{-1}, \quad g = 9.80\ \text{m s}^{-2}, \quad \rho = 9.98 \times 10^2\ \text{kg m}^{-3}, \quad \rho' = 1.205\ \text{kg m}^{-3},$$

$$\nu = 1.004 \times 10^{-6}\ \text{m}^2\ \text{s}^{-1}, \quad \nu' = 1.50 \times 10^{-5}\ \text{m}^2\ \text{s}^{-1}.$$

The characteristic wavenumber and frequency are found to be

$$\bar{k} = 259\ \text{m}^{-1} = \frac{2\pi}{2.4\ \text{cm}}, \qquad \bar{\omega} = 61.7\ \text{s}^{-1} = 2\pi \times 9.8\ \text{Hz},$$

so that the non-dimensional viscosities and density ratio are

$$\frac{\nu\bar{k}^2}{\bar{\omega}} = 1.1 \times 10^{-3}, \qquad \frac{\nu'\bar{k}^2}{\bar{\omega}} = 1.6 \times 10^{-2}, \qquad \frac{\rho'}{\rho} = 1.2 \times 10^{-3}.$$

Thus the steepness has the rough magnitude $\epsilon \approx 0.04$. The implied wave amplitude is $a \sim 0.15$ mm, the implied horizontal wind and drift velocities near the interface are $U'^S \sim 24$ cm s^{-1} and $U^S \sim 1$ cm s^{-1}, and the implied boundary-layer thicknesses are $\epsilon/\bar{k} \sim 0.15$ mm in water and $\mu/\bar{k} \approx 1$ mm in air.

5. Approximate equations for the wave disturbance

From here on all variables are dimensionless unless noted otherwise.

5.1. *Flow equations and boundary conditions for water*

With the introduction of the expansion (4.8), the governing equations for the water flow field can be separated for the interior and the boundary-layer components. For the interior flow field we have

$$\frac{\partial}{\partial t}\nabla^2\psi - \epsilon\frac{\partial(\Psi^S + \psi, \nabla^2(\Psi^S + \psi))}{\partial(x,z)} - \epsilon^2\sigma^2\nabla^4\psi = 0, \tag{5.1}$$

where

$$\sigma^2 = \frac{\nu\bar{k}^2}{\epsilon^2\bar{\omega}} = O(1). \tag{5.2}$$

In the surface boundary layer, we only need to analyse ψ_{BL} up to the leading order because it only appears at the highest orders considered of the kinematic and tangential stress surface conditions due to (4.8),

$$\frac{\partial^2\psi_{BL}}{\partial t\partial z_{BL}} - \frac{\partial\psi}{\partial x}\frac{\partial^2\psi_{BL}}{\partial z_{BL}^2} - \sigma^2\frac{\partial^3\psi_{BL}}{\partial z_{BL}^3} = O(\epsilon). \tag{5.3}$$

The kinematic surface condition and normal stress condition must be accurate to the first three orders. The normal stress from air enters only at $O(\epsilon^2)$ in (2.9). It is defined by (2.6), and will be found after the wave disturbance in air is solved.

The tangential stress condition provides a boundary condition for ψ_{BL}. The tangential stress from air is of relative order ϵ/μ in (2.7), which is too small to be included in the present analysis.

Since the surface boundary-layer thickness is comparable with the wave amplitude $O(\epsilon)$, a new vertical coordinate is introduced which follows the actual position of the free surface:

$$\bar{z}_{BL} = z_{BL} - \eta(t,x). \tag{5.4}$$

In the surface boundary conditions, the interior variables will thus be evaluated at $z = \epsilon\eta$ while the boundary-layer variables will be evaluated at $\bar{z}_{BL} = 0$. The interior variables in the surface conditions can then be Taylor-expanded around the equilibrium surface position $z = 0$, while the boundary-layer variables remain evaluated at the instantaneous surface. The kinematic surface condition then becomes

$$\frac{\partial\eta}{\partial t} + \frac{\partial\psi}{\partial x} + \epsilon\left(U^S\frac{\partial\eta}{\partial x} + \frac{\partial\eta}{\partial x}\frac{\partial\psi}{\partial z} + \eta\frac{\partial^2\psi}{\partial x\partial z}\right) + \epsilon^2\left(\frac{\partial U^S}{\partial z}\eta\frac{\partial\eta}{\partial x} + \frac{\partial\psi_{BL}}{\partial x}\right.$$
$$\left. + \eta\frac{\partial\eta}{\partial x}\frac{\partial^2\psi}{\partial z^2} + \frac{1}{2}\eta^2\frac{\partial^3\psi}{\partial x\partial z^2}\right) = O(\epsilon^3) \quad \text{at} \quad z = 0, \quad \bar{z}_{BL} = 0. \tag{5.5}$$

The normal stress condition becomes

$$\frac{\partial^2\psi}{\partial t\partial z}+\frac{2}{3}\frac{\partial\eta}{\partial x}-\frac{1}{3}\frac{\partial^3\eta}{\partial x^3}+\epsilon\left(-\frac{\partial\psi}{\partial x}\frac{\partial U^S}{\partial z}+\frac{\partial^2\psi}{\partial x\partial z}U^S-\frac{\partial\psi}{\partial x}\frac{\partial^2\psi}{\partial z^2}+\frac{\partial^2\psi}{\partial x\partial z}\frac{\partial\psi}{\partial z}+\eta\frac{\partial^3\psi}{\partial t\partial z^2}\right.$$
$$\left.-\frac{\partial\eta}{\partial x}\frac{\partial^2\psi}{\partial t\partial x}\right)-\epsilon^2\left[\eta\frac{\partial\psi}{\partial x}\frac{\partial^2U^S}{\partial z^2}+\frac{\partial\eta}{\partial x}\frac{\partial^2\psi}{\partial x^2}U^S-\eta\frac{\partial^3\psi}{\partial x\partial z^2}U^S+\eta\frac{\partial\psi}{\partial x}\frac{\partial^3\psi}{\partial z^3}+\sigma^2\frac{\partial^3\psi}{\partial z^3}\right.$$
$$+\frac{\partial\eta}{\partial x}\frac{\partial^2\psi}{\partial x^2}\frac{\partial\psi}{\partial z}-\eta\frac{\partial^3\psi}{\partial x\partial z^2}\frac{\partial\psi}{\partial z}+3\sigma^2\frac{\partial^3\psi}{\partial x^2\partial z}-\frac{\partial\eta}{\partial x}\frac{\partial\psi}{\partial x}\frac{\partial^2\psi}{\partial x\partial z}-\frac{1}{2}\eta^2\frac{\partial^4\psi}{\partial t\partial z^3}+\eta\frac{\partial\eta}{\partial x}\frac{\partial^3\psi}{\partial t\partial x\partial z}$$
$$\left.-\frac{1}{2}\left(\frac{\partial\eta}{\partial x}\right)^2\frac{\partial^3\eta}{\partial x^3}-\frac{\partial\eta}{\partial x}\left(\frac{\partial^2\eta}{\partial x^2}\right)^2+\frac{\partial N}{\partial x}\right]=O(\epsilon^3)\quad\text{at}\quad z=0,\ \bar{z}_{BL}=0. \tag{5.6}$$

The tangential stress condition becomes

$$\frac{\partial^2\psi_{BL}}{\partial\bar{z}_{BL}^2}+\frac{\partial^2\psi}{\partial z^2}-\frac{\partial^2\psi}{\partial x^2}=O\left(\frac{\epsilon}{\mu}\right)\quad\text{at}\quad z=0,\quad\bar{z}_{BL}=0. \tag{5.7}$$

The governing equation for the boundary-layer stream function (5.3) simplifies to

$$\frac{\partial^2\psi_{BL}}{\partial t\partial\bar{z}_{BL}}-\sigma^2\frac{\partial^3\psi_{BL}}{\partial\bar{z}_{BL}^3}=O(\epsilon). \tag{5.8}$$

Finally, the boundary condition at large depth is $\psi\to 0$ as $z\to-\infty$.

To enable further progress, multiple-scale expansions are introduced for the unknowns in water:

$$\eta=\eta_1+\epsilon\eta_2+\epsilon^2\eta_3+\ldots, \tag{5.9}$$
$$\psi=\psi_1+\epsilon\psi_2+\epsilon^2\psi_3+\ldots, \tag{5.10}$$

where all the perturbed quantities depend on the fast coordinates (t,x) and the slow coordinates $t_j=\epsilon^j t$ and $x_j=\epsilon^j x$ for $j=1,2$. These perturbation expansions have been carried out by the symbolic computation tool MACSYMA. Details at each order are given later, when their solutions are discussed.

5.2. *Flow equations and boundary conditions for air*

After substituting (4.4) into the governing equations for the air flow, we get the following equation for the stream function with a truncation error of $O(\epsilon/\mu)$:

$$\frac{\partial}{\partial t}\nabla^2\psi'_w+U'^S\frac{\partial}{\partial x}\nabla^2\psi'_w-\mu\frac{\partial^2U'^S}{\partial z^2}\frac{\partial\psi'_w}{\partial x}-\frac{\epsilon}{\mu^2}\sigma'^2\nabla^4\psi'_w=O\left(\frac{\epsilon}{\mu}\right) \tag{5.11}$$

where

$$\sigma'^2=\frac{\nu'\bar{k}^2}{\epsilon\bar{\omega}}=O(1). \tag{5.12}$$

The presence of the scaling factor μ is due to the boundary-layer component of ψ'_w, according to (4.12).

The no-slip surface boundary conditions can be Taylor-expanded both with respect to the interior and the boundary-layer components because the boundary-layer thickness in air is greater than the surface displacement. After Taylor-expansion, and elimination of terms that only govern the wind profile, we get

$$\frac{\partial\psi'_w}{\partial z}=\frac{\partial\psi}{\partial z}-\frac{\partial U'^S}{\partial z}\eta+O\left(\frac{\epsilon}{\mu}\right)\qquad\text{at}\quad z=0 \tag{5.13}$$

and

$$\frac{\partial \psi'_w}{\partial x} = \frac{\partial \psi}{\partial x} + O(\epsilon) \qquad \text{at} \quad z = 0. \tag{5.14}$$

Finally, we require that the wave disturbance vanishes at great height: $\psi'_w \to 0$ as $z \to \infty$.

After the stream function ψ'_w is solved, the normal stress N for application in (5.6) can be calculated:

$$\frac{\partial N}{\partial x} = \frac{\rho'}{\epsilon^2 \rho} \left\{ \frac{\partial^2 \psi'_w}{\partial t \partial z} + U'^S \frac{\partial^2 \psi'_w}{\partial x \partial z} - \frac{\partial U'^S}{\partial z} \frac{\partial \psi'_w}{\partial x} - \frac{\epsilon}{\mu^2} \sigma'^2 \frac{\partial}{\partial z} \nabla^2 \psi'_w + \frac{2}{3} \frac{\partial \eta}{\partial x} \right\} + O\left(\frac{\epsilon}{\mu}\right) \quad \text{at} \quad z = 0. \tag{5.15}$$

The stream function and normal stress will be solved with a relative truncation error of $O(\epsilon/\mu)$, consistent with neglecting the leading nonlinear effects in air. The perturbation equations are given later, when their solutions are discussed.

6. Wave disturbance in water and evolution equations

With the expansions (5.9) and (5.10), the problems for the interior flow in water (5.1), (5.5) and (5.6) yield a set of perturbation problems with the following general form for all orders m:

$$\frac{\partial}{\partial t} \nabla^2 \psi_m = \mathscr{E}_m \qquad \text{for} \quad -\infty < z < 0, \tag{6.1}$$

$$\frac{\partial \eta_m}{\partial t} + \frac{\partial \psi_m}{\partial x} = \mathscr{F}_m \qquad \text{at} \quad z = 0 \tag{6.2}$$

and

$$\frac{\partial^2 \psi_m}{\partial t \partial z} + \frac{2}{3} \frac{\partial \eta_m}{\partial x} - \frac{1}{3} \frac{\partial^3 \eta_m}{\partial x^3} = \mathscr{G}_m \qquad \text{at} \quad z = 0. \tag{6.3}$$

The forcing functions on the right-hand sides depend on the solutions at lower orders, and for the third order they also depend on the boundary-layer correction and stresses exerted on the surface.

6.1. *First-order problem for water interior*

The first-order problem (6.1)–(6.3) with $m = 1$ is homogeneous, $\mathscr{E}_1 = \mathscr{F}_1 = \mathscr{G}_1 = 0$. The general solution is a progressive wave

$$\eta_1 = \mathscr{A}(t_1, t_2, x_1, x_2) \mathrm{e}^{\mathrm{i}(kx - \omega t)} + \text{c.c.}, \tag{6.4}$$

$$\psi_1 = \frac{\omega}{k} \mathscr{A}(t_1, t_2, x_1, x_2) \mathrm{e}^{\mathrm{i}(kx - \omega t) + kz} + \text{c.c.}, \tag{6.5}$$

subject to the dimensionless dispersion relation

$$\omega^2 = \tfrac{2}{3}k + \tfrac{1}{3}k^3. \tag{6.6}$$

Wilton's ripples correspond to the special solution which is a superposition of a first- and a second-harmonic wave with dimensionless wavenumbers $k = 1$ and $k = 2$. The analysis will be restricted to slow evolution in time only. After introducing the phase function

$$\theta = x - t, \tag{6.7}$$

the leading-order solution for second-harmonic resonance is

$$\eta_1 = A(t_1, t_2)\mathrm{e}^{\mathrm{i}\theta} + B(t_1, t_2)\mathrm{e}^{2\mathrm{i}\theta} + \text{c.c.}, \tag{6.8}$$

$$\psi_1 = A(t_1, t_2)\mathrm{e}^{\mathrm{i}\theta+z} + B(t_1, t_2)\mathrm{e}^{2\mathrm{i}\theta+2z} + \text{c.c.} \tag{6.9}$$

6.2. *Second-order problem for water interior*

The second-order problem (6.1)–(6.3) with $m = 2$ is forced by $\mathscr{E}_2$, $\mathscr{F}_2$ and $\mathscr{G}_2$. They are omitted here for brevity. Owing to quadratic interactions, the solution must be of the form

$$\eta_2 = \hat{\eta}_{2,0} + \hat{\eta}_{2,1}\mathrm{e}^{\mathrm{i}\theta} + \hat{\eta}_{2,2}\mathrm{e}^{2\mathrm{i}\theta} + \hat{\eta}_{2,3}\mathrm{e}^{3\mathrm{i}\theta} + \hat{\eta}_{2,4}\mathrm{e}^{4\mathrm{i}\theta} + \text{c.c.}, \tag{6.10}$$

$$\psi_2 = \hat{\psi}_{2,0} + \hat{\psi}_{2,1}\mathrm{e}^{\mathrm{i}\theta} + \hat{\psi}_{2,2}\mathrm{e}^{2\mathrm{i}\theta} + \hat{\psi}_{2,3}\mathrm{e}^{3\mathrm{i}\theta} + \hat{\psi}_{2,4}\mathrm{e}^{4\mathrm{i}\theta} + \text{c.c.} \tag{6.11}$$

The governing equations at the second order give no contribution for the zeroth-harmonic, hence $\hat{\eta}_{2,0}(t_1, t_2)$ and $\hat{\psi}_{2,0}(t_1, t_2, z)$ remain undetermined. The problems for each of the remaining harmonics have the general form for order $m = 2$ and harmonics $n = 1, 2, 3, 4$:

$$\frac{\partial^2\hat{\psi}_{m,n}}{\partial z^2} - n^2\hat{\psi}_{m,n} = E_{m,n}\mathrm{e}^{nz} \qquad \text{for} \quad -\infty < z < 0, \tag{6.12}$$

$$\hat{\eta}_{m,n} - \hat{\psi}_{m,n} = F_{m,n} \qquad \text{at} \quad z = 0, \tag{6.13}$$

$$\frac{\partial\hat{\psi}_{m,n}}{\partial z} - \frac{n^2+2}{3}\hat{\eta}_{m,n} = G_{m,n} \qquad \text{at} \quad z = 0. \tag{6.14}$$

The forcing terms $E_{2,n}, F_{2,n}, G_{2,n}$ are omitted for brevity.

We have chosen to let the homogeneous part of the solutions to the first- and second-harmonic problems correspond to $\hat{\eta}_{2,1} = \hat{\eta}_{2,2} = 0$. The solvability conditions for these problems take the form

$$\int_{-\infty}^{0} \mathrm{e}^{2nz}E_{2,n}\,\mathrm{d}z = nF_{2,n} + G_{2,n}, \qquad n = 1, 2, \tag{6.15}$$

and yield the slow evolution equations

$$\frac{\partial A}{\partial t_1} + 2\mathrm{i}A\int_{-\infty}^{0} \mathrm{e}^{2z}U^S(z)\,\mathrm{d}z + \mathrm{i}A^*B = 0 \tag{6.16}$$

and

$$\frac{\partial B}{\partial t_1} + 8\mathrm{i}B\int_{-\infty}^{0} \mathrm{e}^{4z}U^S(z)\,\mathrm{d}z + \tfrac{1}{2}\mathrm{i}A^2 = 0. \tag{6.17}$$

The integral terms give phase shifts induced by the shear current in water.

6.3. *Surface boundary layer in water*

The surface boundary layer is governed by (5.8) with tangential stress boundary condition (5.7). The leading-order boundary-layer problem is linear, hence we assume a solution of the form

$$\psi_{BL} = \hat{\psi}_{BL,1}\mathrm{e}^{\mathrm{i}\theta} + \hat{\psi}_{BL,2}\mathrm{e}^{2\mathrm{i}\theta} + \text{c.c.} \tag{6.18}$$

For compactness we write $\mathscr{A}_1 = A$ and $\mathscr{A}_2 = B$ for the time being; the first- and second-harmonic boundary-layer problems are for $n = 1, 2$

$$n\frac{\partial\hat{\psi}_{BL,n}}{\partial\bar{z}_{BL}} - \mathrm{i}\sigma^2\frac{\partial^3\hat{\psi}_{BL,n}}{\partial\bar{z}_{BL}^3} = 0 \qquad \text{for} \quad -\infty < \bar{z}_{BL} < 0, \tag{6.19}$$

$$\frac{\partial^2 \hat{\psi}_{BL,n}}{\partial \bar{z}_{BL}^2} = -2n^2 \mathscr{A}_n \qquad \text{at} \quad \bar{z}_{BL} = 0. \tag{6.20}$$

The solutions are

$$\hat{\psi}_{BL,n} = -2\mathrm{i}\sigma^2 n \mathscr{A}_n \exp(-n^{1/2}\sigma^{-1}\mathrm{e}^{-\mathrm{i}\pi/4}\bar{z}_{BL}), \qquad n = 1, 2. \tag{6.21}$$

6.4. *Third-order problem for water interior*

The third-order problem, (6.1)–(6.3) with $m = 3$, has lengthy right-hand sides $\mathscr{E}_3$, $\mathscr{F}_3$ and $\mathscr{G}_3$. They are omitted here for brevity. For third-order improvement of the evolution equations for A and B, we need the zeroth-harmonic of the second-order problem, and to invoke the solvability of the first- and second-harmonic problems. It is enough to look at

$$\eta_3 = \hat{\eta}_{3,1}\mathrm{e}^{\mathrm{i}\theta} + \hat{\eta}_{3,2}\mathrm{e}^{2\mathrm{i}\theta} + \ldots, \tag{6.22}$$

$$\psi_3 = \hat{\psi}_{3,1}\mathrm{e}^{\mathrm{i}\theta} + \hat{\psi}_{3,2}\mathrm{e}^{2\mathrm{i}\theta} + \ldots. \tag{6.23}$$

We also expand formally the normal stress on the sea surface into harmonics:

$$N = \hat{N}_1 A\mathrm{e}^{\mathrm{i}\theta} + \hat{N}_2 B\mathrm{e}^{2\mathrm{i}\theta} + \text{c.c.} \tag{6.24}$$

The computation of the normal stress awaits the solution of the air problem in the next section.

The zeroth-harmonic problem, which governs the zeroth-harmonic quantities introduced at the second order, is not forced:

$$\frac{\partial^3 \hat{\psi}_{2,0}}{\partial t_1 \partial z^2} = 0, \qquad \text{with} \qquad \frac{\partial \hat{\eta}_{2,0}}{\partial t_1} = 0 \quad \text{and} \quad \frac{\partial^2 \hat{\psi}_{2,0}}{\partial t_1 \partial z} = 0 \quad \text{at} \quad z = 0. \tag{6.25}$$

We therefore set $\hat{\psi}_{2,0} = \hat{\eta}_{2,0} = 0$.

The problems for order $m = 3$ and harmonics $n = 1, 2$ are given by (6.12)–(6.14). The expressions for $E_{3,n}$, $F_{3,n}$ and $G_{3,n}$ are long, and are not given here.

Invoking solvability of the inhomogeneous problems for $n = 1, 2$, we get

$$\frac{\partial A}{\partial t_2} + (d_1 + \mathrm{i}a_{11})A + 10\mathrm{i}cA^*B + \mathrm{i}A|A|^2 - \tfrac{21}{2}\mathrm{i}A|B|^2 = 0 \tag{6.26}$$

and

$$\frac{\partial B}{\partial t_2} + (d_2 + \mathrm{i}a_{21})B + \tfrac{9}{2}\mathrm{i}cA^2 - \tfrac{41}{4}\mathrm{i}B|A|^2 - 4\mathrm{i}B|B|^2 = 0. \tag{6.27}$$

Use has been made of (6.16) and (6.17) to remove the derivatives with respect to t_1. The coefficients a_{n1} and c depend on the shear current in the water, while the coefficients d_n depend on viscous shear in water and the wave disturbance in air.

6.5. *Summary of the slow evolution equations for Wilton's ripples*

We can now combine (6.16)–(6.17) and (6.26)–(6.27) to get the evolution equations valid for time $t_1 = O(\epsilon^{-1})$†. The results are

$$\frac{\partial A}{\partial t_1} + \{\epsilon d_1 + \mathrm{i}(a_{10} + \epsilon a_{11})\}A + \mathrm{i}\{1 + 10\epsilon c\}A^*B + \mathrm{i}\epsilon A|A|^2 - \tfrac{21}{2}\mathrm{i}\epsilon A|B|^2 = 0 \tag{6.28}$$

† Jones (1992) derived an analogous system of two coupled cubic nonlinear Schrödinger equations for the case of no wind, shear current or viscosity, but included general spatial modulation on scales x_1 and y_1. In the inviscid and windless limit, our evolution equations agree with Jones', after minor corrections.

and

$$\frac{\partial B}{\partial t_1} + \{\epsilon d_2 + \mathrm{i}\,(a_{20} + \epsilon a_{21})\}\,B + \mathrm{i}\left\{\tfrac{1}{2} + \tfrac{9}{2}\epsilon c\right\} A^2 - \tfrac{41}{4}\mathrm{i}\epsilon B|A|^2 - 4\mathrm{i}\epsilon B|B|^2 = 0. \quad (6.29)$$

The coefficients that depend on the shear current in water are for $n = 1, 2$

$$a_{n0} = 2n^2 \int_{-\infty}^{0} \mathrm{e}^{2nz} U^S(z)\,\mathrm{d}z, \quad (6.30)$$

$$a_{n1} = n^2 \int_{-\infty}^{0} \mathrm{e}^{2nz} \left(U^S(z)\right)^2 \mathrm{d}z - 2n^3 \left(\int_{-\infty}^{0} \mathrm{e}^{2nz} U^S(z)\,\mathrm{d}z\right)^2, \quad (6.31)$$

$$c = 2\int_{-\infty}^{0} \mathrm{e}^{4z} U^S(z)\,\mathrm{d}z - \int_{-\infty}^{0} \mathrm{e}^{2z} U^S(z)\,\mathrm{d}z. \quad (6.32)$$

The complex coefficients that account for viscous damping and linear normal stress from air on the water surface are

$$d_n = 2n^2\sigma^2 - \tfrac{1}{2}\mathrm{i}\hat{N}_n, \qquad n = 1, 2. \quad (6.33)$$

The complex coefficients $\hat{N}_n$, which depend on the wave disturbance in air, will be derived in §7.

Our approximate theory has only two independent parameters: (i) the typical wave steepness ϵ, and (ii) the wind intensity, given in terms of the friction velocity in air u'_*.

It is shown in the Appendix that the total energy is

$$E = 2(|A|^2 + 2|B|^2) + 2\epsilon(a_{10}|A|^2 + a_{20}|B|^2) + \epsilon\,\mathrm{Re}(A^2B^*). \quad (6.34)$$

6.6. *Reduction of dimension*

The dynamical system (6.28)–(6.29) has four real dimensions, which can be reduced to three by using the fact that the phase angles appear only as a difference. To this end we rewrite the complex amplitudes in polar form

$$A = \mathscr{U}\mathrm{e}^{\mathrm{i}\theta_1}, \qquad B = \mathscr{V}\mathrm{e}^{\mathrm{i}\theta_2}, \qquad \phi = 2\theta_1 - \theta_2. \quad (6.35)$$

However, we find it more convenient to work in rectangular than polar coordinates, and thus following Vyshkind & Rabinovich (1976), we introduce the transformed variables

$$X = \mathscr{V}\cos\phi, \qquad Y = \mathscr{V}\sin\phi, \qquad Z = \mathscr{U}^2. \quad (6.36)$$

Hence Z is non-negative and measures the square of the amplitude of the first harmonic. The radial distance from the Z-axis, $(X^2 + Y^2)^{1/2}$, is a measure of the second-harmonic amplitude. The dynamics is confined to the upper half of the (XYZ)-space.

The dynamical system now becomes

$$\frac{\mathrm{d}X}{\mathrm{d}t_1} = -\epsilon d_{2,R}X - \alpha_3 Y - 2\alpha_1 XY + \tfrac{49}{4}\epsilon YZ - 17\epsilon(X^2 + Y^2)Y, \quad (6.37)$$

$$\frac{\mathrm{d}Y}{\mathrm{d}t_1} = \alpha_3 X - \epsilon d_{2,R}Y + \alpha_2 Z + 2\alpha_1 X^2 - \tfrac{49}{4}\epsilon XZ + 17\epsilon X(X^2 + Y^2), \quad (6.38)$$

$$\frac{\mathrm{d}Z}{\mathrm{d}t_1} = -2\epsilon d_{1,R}Z + 2\alpha_1 YZ. \quad (6.39)$$

Note that when $Z = 0$, only the second harmonic is present.

The coefficients α_n are given by

$$\alpha_1 = -1 - 10\epsilon c, \qquad \alpha_2 = \tfrac{1}{2} + \tfrac{9}{2}\epsilon c \tag{6.40}$$

and

$$\alpha_3 = -2a_{10} + a_{20} + \epsilon\left(-2a_{11} + a_{21} - 2d_{1,I} + d_{2,I}\right). \tag{6.41}$$

We have split the linear forcing coefficients d_n into real and imaginary parts

$$d_n = d_{n,R} + \mathrm{i}d_{n,I}, \qquad n = 1, 2. \tag{6.42}$$

The energy (6.34) is now expressed by

$$E = 4(X^2 + Y^2) + 2Z + \epsilon\left(XZ + 2a_{20}(X^2 + Y^2) + 2a_{10}Z\right). \tag{6.43}$$

7. Wave disturbance in air

To complete the evolution equations, we must find the air motion in order to calculate the stresses on the sea surface. The linear problem in air, which is generic for all wavenumbers, is solved for an arbitrary simple-harmonic wave. The explicit orderings in terms of ϵ and μ are omitted in this section for brevity.

7.1. *Linear problem in air for a simple-harmonic wave*

At the leading order, the wave disturbance in water is given by (6.4)–(6.5). The corresponding disturbance in air must be of the form

$$\psi' = \hat{\psi}'_k(z)\mathscr{A}\mathrm{e}^{\mathrm{i}(kx-\omega t)} + \text{c.c.}, \tag{7.1}$$

$$N = \hat{N}_k\mathscr{A}\mathrm{e}^{\mathrm{i}(kx-\omega t)} + \text{c.c.} \tag{7.2}$$

From (5.11), $\hat{\psi}'_k$ can be shown to obey the homogeneous Orr–Sommerfeld equation

$$\left[\omega - kU'^S - \mathrm{i}\sigma'^2\left(\frac{\partial^2}{\partial z^2} - k^2\right)\right]\left(\frac{\partial^2}{\partial z^2} - k^2\right)\hat{\psi}'_k + k\frac{\partial^2 U'^S}{\partial z^2}\hat{\psi}'_k = 0 \tag{7.3}$$

with the inhomogeneous boundary conditions (5.13)–(5.14)

$$\hat{\psi}'_k = \frac{\omega}{k} \qquad \text{and} \qquad \frac{\partial\hat{\psi}'_k}{\partial z} = \omega - \frac{\partial U'^S}{\partial z} \qquad \text{at} \quad z = 0. \tag{7.4}$$

From (6.28) and (6.29) we see that the net growth rate of the simple-harmonic wave is given by the real part of $-d_n$ in (6.33) generalized to arbitrary wavenumbers:

$$\mathrm{Re}\left\{-2k^2\sigma^2 + \frac{\mathrm{i}k}{2\omega}\hat{N}_k\right\}. \tag{7.5}$$

The first term in the braces represents internal viscous dissipation, while the second term represents forcing by the normal stress

$$\hat{N}_k = \frac{\rho'}{\rho}\left\{-\frac{\partial U'^S}{\partial z}\hat{\psi}'_k - \left(\frac{\omega}{k} - U'^S + \mathrm{i}k\sigma'^2\right)\frac{\partial\hat{\psi}'_k}{\partial z} + \frac{\mathrm{i}\sigma'^2}{k}\frac{\partial^3\hat{\psi}'_k}{\partial z^3} + \frac{2}{3}\right\}. \tag{7.6}$$

Using the solution for $k = 1, 2$, we obtain the linear response in air according to

$$\psi' = \hat{\psi}'_1 A\mathrm{e}^{\mathrm{i}\theta} + \hat{\psi}'_2 B\mathrm{e}^{2\mathrm{i}\theta} + \text{c.c.}, \tag{7.7}$$

$$N = \hat{N}_1 A\mathrm{e}^{\mathrm{i}\theta} + \hat{N}_2 B\mathrm{e}^{2\mathrm{i}\theta} + \text{c.c.} \tag{7.8}$$

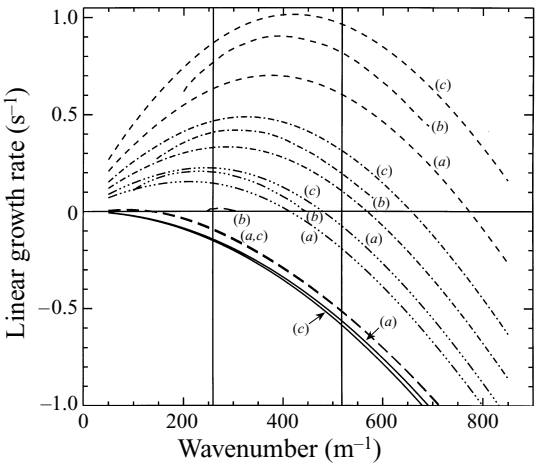

FIGURE 1. Linear growth rates: (*a*) our result; (*b*) asymptotic result of Gastel *et al.* (1985); (*c*) our result including tangential stress (Trulsen 1995). Air friction velocity u'_* (m s^{-1}): - - -, 0.214; -·-·-, 0.170; - · · ·, 0.136; — — —, 0.050; solid line, no wind. The vertical lines indicate the first- and second-harmonic Wilton's ripples.

7.2. *Computed growth rates*

In figure 1 our linear growth rates predicted by (7.5) for four wind intensities are shown by the curves (*a*). The limit of no wind is shown by the lower solid curve. For comparison the asymptotic growth rates inferred from Gastel *et al.* (1985) are also shown, by the curves (*b*). Except for the weakest wind, our predictions are only slightly lower. The significant discrepancy for the weakest wind is because they assumed that the two wave-induced viscous shear layers in air, i.e. the surface boundary layer and the critical shear layer, overlap and can be treated as a single boundary layer. This assumption is violated for vanishing winds, as discussed in §4.

More accurate computations incorporating effects of relative order ϵ/μ in air were carried out in Trulsen (1995), allowing the effect of tangential stress to be assessed. These results are shown by the curves (*c*). The tangential stress contributes to a larger growth rate for air friction velocities larger than roughly 0.05 m s^{-1}, while it contributes to stronger damping for friction velocities smaller than roughly 0.04 m s^{-1}.

In figure 2 we show the real and imaginary parts of the linear coefficients d_1 and d_2, equation (6.33), for air friction velocities up to 0.17 m s^{-1}. The linear growth rates for the first and second harmonics of Wilton's ripples are given by $-\operatorname{Re} d_1$ and $-\operatorname{Re} d_2$.

We are interested long-time evolution subject to viscous damping and wind forcing. Intuitively, one of the harmonics must then be growing and the other must be damped. We can anticipate from figure 1 that energy must be added to the first-harmonic wave, then transferred to the second-harmonic wave through nonlinear interaction, and finally dissipated from the second-harmonic wave.

8. Recapitulation of second-order behaviour

In the limit of $\epsilon \to 0$, the second-order conservative behaviour of Wilton's ripples is well known (McGoldrick 1965, 1970; Simmons 1969; Chen & Saffman 1979). As a reference for later analysis of the third-order system (6.37)–(6.39), it is convenient to review the key results of the reduced system in terms of the present (X, Y, Z)

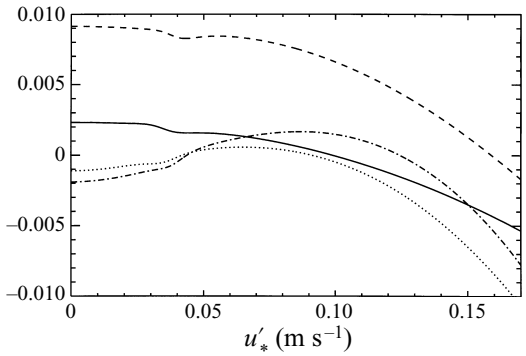

FIGURE 2. Linear coefficients d_1 and d_2, equation (6.33).
—, Re d_1; ···, Im d_1; – –, Re d_2; – · – ·, Im d_2.

variables, i.e.

$$\dot{X} = -\alpha_{30} Y + 2XY, \tag{8.1}$$

$$\dot{Y} = \alpha_{30} X + \tfrac{1}{2} Z - 2X^2, \tag{8.2}$$

$$\dot{Z} = -2YZ. \tag{8.3}$$

The only controlling parameter is

$$\alpha_{30} = -2a_{10} + a_{20} \tag{8.4}$$

which includes the Doppler effect of surface drift. The second-order energy is conserved, and is given by

$$E_0 = 4(X^2 + Y^2) + 2Z = \text{constant}. \tag{8.5}$$

The constancy of energy confines the dynamical behaviour to an elliptic paraboloid in the (X, Y, Z)-space. Upon eliminating Z with the help of (8.5), we get the Hamiltonian system

$$\dot{X} = -\alpha_{30} Y + 2XY = \frac{\partial H}{\partial Y}, \tag{8.6}$$

$$\dot{Y} = \alpha_{30} X - 3X^2 - Y^2 + \tfrac{1}{4} E_0 = -\frac{\partial H}{\partial X}, \tag{8.7}$$

with

$$H(X, Y) = -\tfrac{1}{2}\alpha_{30}(X^2 + Y^2) + X(X^2 + Y^2 - \tfrac{1}{4} E_0). \tag{8.8}$$

The trajectories on the elliptic paraboloid can therefore be obtained by computing the level-curves of H.

One of the fixed points of the second-order system is in the (X, Y)-plane with $Z = 0$. This implies that a pure second-harmonic wave is a steady-state solution. For $Z > 0$ there are at most two fixed points (X_c, Y_c, Z_c) defined by

$$3X_c^2 - \alpha_{30} X_c - \tfrac{1}{4} E_0 = 0, \qquad Y_c = 0, \qquad Z_c = 4X_c^2 - 2\alpha_{30} X_c. \tag{8.9a,b,c}$$

By linearization, the fixed points (X_c, Y_c, Z_c) can be shown to be centres on the surface of the elliptic paraboloid. The second-order conservative system has in fact a continuum of centres along the parts of the parabola (8.9*b*,*c*) standing above the (X, Y)-plane.

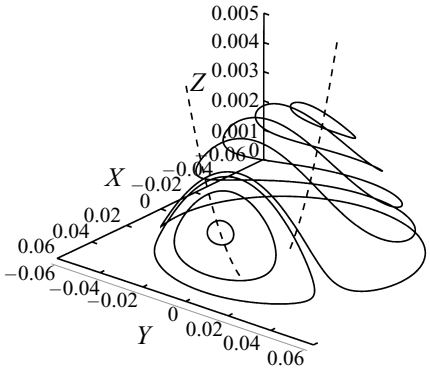

FIGURE 3. Trajectories of second-order system for $u'_* = 0.1$ m s^{-1} ($\alpha_{30} = 0.0572$) and $E_0 = 0.01$ (—). The parabola of fixed points (with $Z > 0$) indicates the locations of the centres (- - -).

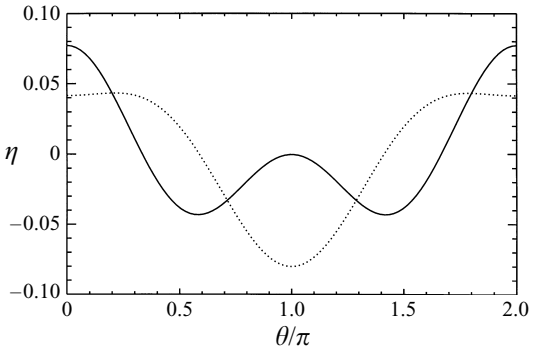

FIGURE 4. Wave profiles for the steady-state solutions at the centres for $u'_* = 0.1$ m s^{-1} ($\alpha_{30} = 0.0572$) and $E_0 = 0.01$: —, gravity type; $\cdots$, capillary type.

In figure 3 we show three-dimensional trajectories of the second-order system by solid curves for one specific energy level $E_0 = 0.01$ and for $u'_* = 0.1$ m s^{-1}. This implies that $\alpha_{30} = 0.0572$ according to (6.41). The parabola of fixed points is shown by a dashed curve for $Z > 0$. The orbits are seen to be located on an elliptic paraboloid.

In figure 4 we show one wave period of the surface elevation $\eta = \eta_1$, equation (6.8), corresponding to the steady-state solutions at the two centres. We have again set $E_0 = 0.01$ and $u'_* = 0.1$ m s^{-1}. The phase angle is arbitrarily set to zero $\theta_1 = 0$; the exact choice is immaterial since it only affects a trivial phase shift and not the shape of the wave.

9. Third-order behaviour

The full dynamical system (6.37)–(6.39) will now be discussed. In the figures that follow we set $\epsilon = \mu = 1$, and let the dynamical variables have proper magnitudes consistent with the assumed scales. In particular A, B, X and Y must be $O(\epsilon)$ while Z and the energy E must be $O(\epsilon^2)$. In the following we thus limit our numerical discussion to $X, Y = O(0.1)$ and $Z, E = O(0.01)$.

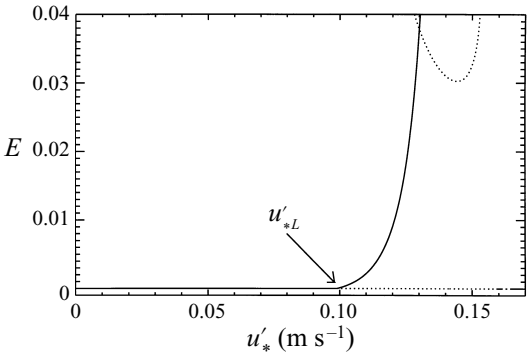

FIGURE 5. The stability of fixed points: —, stable; ···, one unstable eigenvalue; – · – ·, three unstable eigenvalues.

9.1. *Fixed points and their stability*

From (6.39) we note that if $Z = 0$ initially, then $Z = 0$ for all time. This implies that a pure second-harmonic wave is a steady-state solution.

The only fixed point in the (X, Y)-plane is the origin $X = Y = Z = 0$. The stability of the origin can be analysed by considering the linearized system

$$\frac{\mathrm{d}}{\mathrm{d}t_1}\begin{pmatrix} X \\ Y \\ Z \end{pmatrix} = \begin{pmatrix} -\epsilon d_{2,R} & -\alpha_3 & 0 \\ \alpha_3 & -\epsilon d_{2,R} & \alpha_2 \\ 0 & 0 & -2\epsilon d_{1,R} \end{pmatrix}\begin{pmatrix} X \\ Y \\ Z \end{pmatrix}. \tag{9.1}$$

It follows that the (X, Y)-plane is an eigenspace with two complex conjugate eigenvalues $\lambda = -\epsilon d_{2,R} \pm \mathrm{i}\alpha_3$. The motion in the (X, Y)-plane is hence spiralling either into or away from the origin. There is also an eigenvalue $\lambda = -2\epsilon d_{1,R}$ with an eigenvector going out of the (X, Y)-plane.

For weak winds such that the first and second harmonics are linearly damped ($d_{1,R} > 0$, $d_{2,R} > 0$), the origin is a stable fixed point. For intermediate winds such that the first harmonic is linearly growing ($d_{1,R} < 0$) and the second harmonic is linearly damped ($d_{2,R} > 0$), the origin is unstable along the eigendirection out of the (X, Y)-plane, but is stable with inward spiralling motion in the (X, Y)-plane. For stronger winds such that both harmonics are linearly growing, the origin is unstable in all directions.

Next we look for fixed points with $Z > 0$. They are determined by setting the right-hand sides in (6.37)–(6.39) equal to zero. For a given solution for X, we then find that

$$Y \approx -\epsilon d_{1,R}, \qquad Z \approx 4X^2 - 2\alpha_{30}X. \tag{9.2}$$

It is evident that these fixed points are located approximately on the parabola of centres (8.9) found for the second-order conservative system. For a solution to be acceptable, the resulting value of Z must be non-negative, and the magnitudes must also be within the assumed bounds.

We have computed numerically the fixed points and their stability. Figure 5 shows a bifurcation diagram in terms of the energy E versus the air friction velocity u'_*. In order to stay in the range of validity of our theory, only results with $E = O(\epsilon^2)$ are plotted. The stability of the fixed points is indicated with different line styles depending on the number of stable eigenvalues, as explained in the figure. There is a fixed point with no energy $E = 0$ corresponding to no wave disturbance. This fixed

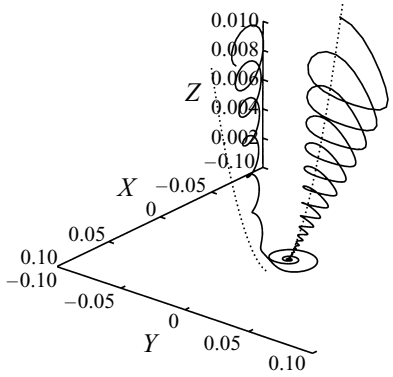

FIGURE 6. Two trajectories for $u'_* = 0.08$ m s^{-1}. Initial conditions $(-0.05, 0, 0.015)$ and $(0.05, 0, 0.015)$. Stable fixed point at the origin (0, 0, 0).

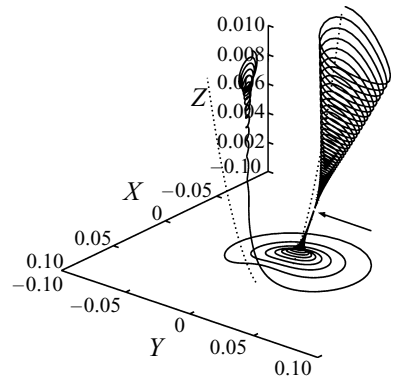

FIGURE 7. Two trajectories for $u'_* = 0.12$ m s^{-1}. Initial conditions $(-0.05, 0, 0.016)$ and $(0.04, 0, 0.016)$. The stable fixed point at $(-0.019, 0.0010, 0.0030)$ can be seen as the gap in the trajectory, indicated by the arrow.

stable fixed point. From another initial point $(0.04, 0, 0.016)$ the trajectory first spirals down along the branch of the parabola (8.9) with positive X. As it approaches the (X, Y)-plane, it is at first trapped in the inward spiralling motion toward the origin, but is then ejected up toward the stable fixed point. Thus both initial states lead to Wilton's ripples of permanent form.

Finally we examine a relatively strong wind with $u'_* = 0.17$ m s^{-1} which is in wind range (iii) with both the first and second harmonics linearly growing. In figure 8 the origin is an unstable fixed point. From the initial point $(0.02, 0, 0.000001)$ the trajectory first spirals away from the origin close to the (X, Y)-plane, signifying the slow growth of the second harmonic. It is then ejected away from the (X, Y)-plane, and becomes unbounded in Z, indicating rapid growth of the first harmonic.

The behaviour shown in figure 8 is qualitatively similar to the experimental observation of Choi (1977) and Ramamonjiarisoa *et al.* (1978) and the numerical result of Janssen (1987): at first a second-harmonic wave grows slowly due to wind, then the peak of the spectrum is suddenly shifted to a rapidly growing first-harmonic wave. However, as our theory breaks down due to blow-up, the experiment suggests that the spectrum actually becomes broad-banded.

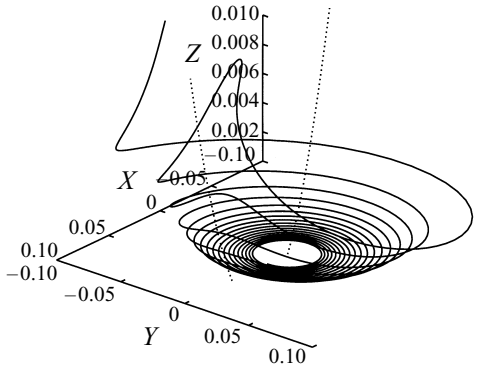

FIGURE 8. One trajectory for $u'_* = 0.17$ m s^{-1}. One initial condition $(0.02, 0, 0.000001)$.

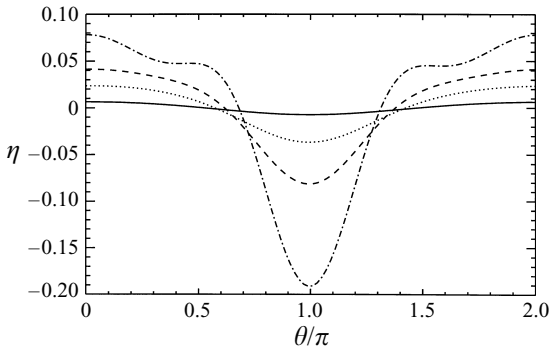

FIGURE 9. Wave profiles for the stable steady-state solution for various wind speeds u'_*: —, 0.10 m s^{-1}; $\cdots$, 0.11 m s^{-1}; – –, 0.12 m s^{-1}; – $\cdot$ – $\cdot$, 0.13 m s^{-1}.

All our numerical experience in wind range (iii) suggests that the total wave energy will grow out of bounds, i.e. blow-up.

9.3. *The steady Wilton's ripples*

Because the stable non-trivial fixed point in wind range (ii) lies close to the parabola of centres of the second-order system, it is mathematically similar to a special case of the steady progressive waves found by Wilton (1915) and Pierson & Fife (1961). However, the present theory gives information on the wind conditions under which these waves are likely observable in reality.

In figure 9 we show one wave period of the surface elevation $\eta = \eta_1 + \epsilon\eta_2$, equations (6.8) and (6.10), of the stable progressive waves with permanent form.

According to our results, Wilton's ripples can sustain viscous damping if the air friction velocity is roughly in the range 0.09–0.13 m s^{-1}. From empirical relations between the air friction velocity u'_* and the reference wind speed, the threshold wind speed for Wilton's ripples to exist can be estimated. For example, Shemdin (1972) reported that the friction velocity was 4.95% of the reference wind speed. Janssen (1986) used the values 4.0% and 4.28% for application to the experiment of Choi (1977). Klinke & Jähne (1992) found the ratio to be 4.90%. Based on these estimates, the minimum wind speeds for steady Wilton's ripples in dynamical equilibrium with wind and viscosity should be roughly 2–3 m s^{-1}, which is a light breeze on the Beaufort scale.

Strizhkin & Raletnev (1986) observed resonating triads on the sea surface for reference wind speeds above 2.7 m s^{-1}. This is clearly within our theoretical range, being close to the boundary between wind ranges (ii) and (iii) of our theory.

10. Concluding remarks

To supplement existing theories on inviscid and wind-free gravity–capillary waves which are difficult to produce in the laboratory or nature, we have developed a theory for second-harmonic resonance of Wilton's ripples under the influence of weak wind. Limiting to slow modulation in time only, we have shown that there are essentially three qualitatively different types of behaviour depending on the wind speed. For winds weaker than a lower threshold, both the first- and the second-harmonic waves are linearly damped and wave disturbances die out. For winds stronger than the lower threshold, but weaker than an upper threshold, stable waves of permanent form exist where nonlinearity, wind forcing and viscous damping are in dynamical equilibrium. Thus we have shown that the steady inviscid ripples described by Wilton (1915) can in fact be stable under certain conditions.

For still stronger winds, above the upper threshold, the total wave energy grows without bound. Blow-up is known to occur for non-conservative second-order resonant systems that have been truncated at the quadratic nonlinear order, and can occur even when one of the waves is linearly damped. Previous authors (e.g. McDougall & Craik 1991) have anticipated that such singular behaviour could be arrested by including cubic nonlinear interactions. We have however shown that blow-up can occur even when cubic nonlinear interactions are included. During the limited time of evolution before the blow-up, the qualitative tendency of period doubling of phase oscillations is similar to that observed experimentally by Choi (1977) and theoretically by Janssen (1986, 1987) for relatively strong wind. Analysis of blow-up would require a theory allowing the development of a broad-banded spectrum as in Janssen (1987).

Other extensions of this work on triad resonance appear desirable: (i) the effects of wind and viscosity when the three component waves are in different directions, (ii) slow evolution in both time and space, and (iii) the effects of longer gravity waves. Progress in one or all of these aspects will further enhance our understanding of small-scale processes on the sea surface.

This research has been supported by the US Office of Naval Research (N00014–92J–1754), the US National Science Foundation (CTS–9115689) and the Norwegian Research Council (NFR 109328/410).

Appendix. Energy of Wilton's ripples correct to the third order

In dimensional variables, the wave kinetic energy is

$$E_k = \overline{\int_{-\infty}^{\eta} \frac{\rho}{2} \left\{ \left(\frac{\partial \psi}{\partial x} \right)^2 + \left(\frac{\partial \psi}{\partial z} \right)^2 + 2 \frac{\partial \Psi^S}{\partial z} \frac{\partial \psi}{\partial z} \right\} \mathrm{d}z}, \tag{A 1}$$

the wave gravitational potential energy is

$$E_g = \overline{\int_{-\infty}^{\eta} \rho g z \, \mathrm{d}z}, \tag{A 2}$$

and the wave surface potential energy is

$$E_\Gamma = \overline{\Gamma \left\{ \left(1 + \left(\frac{\partial \eta}{\partial x} \right)^2 \right)^{1/2} - 1 \right\}}. \tag{A 3}$$

In the non-dimensional variables of §6, the kinetic energy becomes

$$E_k = \frac{1}{2} \int_{-\infty}^{0} \overline{\left\{ \left(\frac{\partial \psi}{\partial x} \right)^2 + \left(\frac{\partial \psi}{\partial z} \right)^2 \right\}} \, \mathrm{d}z + \epsilon \tfrac{1}{2} \overline{\eta \left\{ \left(\frac{\partial \psi}{\partial x} \right)^2 + \left(\frac{\partial \psi}{\partial z} \right)^2 \right\}_{z=0}} \tag{A 4}$$

while the total potential energy becomes

$$E_p = E_g + E_\Gamma = \tfrac{1}{3} \overline{\eta^2} + \frac{1}{6} \overline{\left(\frac{\partial \eta}{\partial x} \right)^2}. \tag{A 5}$$

Hence the total energy is

$$E = E_k + E_p = 2(|A|^2 + 2|B|^2) + 2\epsilon(a_{10}|A|^2 + a_{20}|B|^2) + \epsilon \, \mathrm{Re}(A^2 B^*). \tag{A 6}$$

REFERENCES

Bontozoglou, V. & Hanratty, T. J. 1990 Capillary–gravity Kelvin–Helmholtz waves close to resonance. *J. Fluid Mech.* **217**, 71–91.

Chen, B. & Saffman, P. G. 1979 Steady gravity-capillary waves in deep water — I. Weakly nonlinear waves. *Stud. Appl. Maths* **60**, 183–210.

Choi, I. 1977 Contributions a l'étude des mecanismes physiques de la génération des ondes de capillarité-gravité à une interface air-eau. Thesis, Université d'Aix Marseille.

Chow, C. C., Bers. A. & Ram, A. K. 1992 The three wave interaction and spatiotemporal chaos. *Physics of Space Plasmas (1991)* (ed. T. Chang, G. B. Crew & J. R. Jasperse). SPI Conf. Proc. and Reprint Series, Number 11, pp. 179–195. Scientific Publishers, Inc., Cambridge, MA.

Christodoulides, P. & Dias, F. 1994 Resonant capillary-gravity interfacial waves. *J. Fluid Mech.* **265**, 303–343.

Craik, A. D. D. 1986 Exact solutions of non-conservative equations for three-wave and second-harmonic resonance. *Proc. R. Soc. Lond.* A **406**, 1–12.

Gastel, K. van, Janssen, P. A. E. M. & Komen, G. J. 1985 On phase velocity and growth rate of wind-induced gravity-capillary waves. *J. Fluid Mech.* **161**, 199–216.

Hara, T. & Mei, C. C. 1994 Wind effects on the nonlinear evolution of slowly varying gravity-capillary waves. *J. Fluid Mech.* **267**, 221–250.

Harrison, W. J. 1909 The influence of viscosity and capillarity on waves of finite amplitude. *Proc. Lond. Math. Soc.* **7**, 107–121.

Hughes, D. W. & Proctor, M. R. E. 1992 Nonlinear three-wave interaction with non-conservative coupling. *J. Fluid Mech.* **244**, 583–604.

Janssen, P. A. E. M. 1986 The period-doubling of gravity–capillary waves. *J. Fluid Mech.* **172**, 531–546.

Janssen, P. A. E. M. 1987 The initial evolution of gravity–capillary waves. *J. Fluid Mech.* **184**, 581–597.

Jones, M. C. W. 1992 Nonlinear stability of resonant capillary-gravity waves. *Wave Motion* **15**, 267–283.

Jurman, L. A., Deutsch, S. E. & McCready, M. J. 1992 Interfacial mode interactions in horizontal gas–liquid flows. *J. Fluid Mech.* **238**, 187–219.

Kawai, S. 1979 Generation of initial wavelets by instability of a coupled shear flow and their evolution to wind waves. *J. Fluid Mech.* **93**, 661–703.

Klinke, J. & Jähne, B. 1992 2D wave number spectra of short wind waves — results from wind wave facilities and extrapolation to the ocean. In *Optics of the Air-Sea Interface: Theory and Measurements* (ed. L. Estep). SPIE 1749, pp. 245–257.

McDougall, S. R. & Craik, A. D. D. 1991 Blow-up in non-conservative second-harmonic resonance. *Wave Motion* **13**, 155–165.

McGoldrick, L. F. 1965 Resonant interactions among capillary-gravity waves. *J. Fluid Mech.* **21**, 305–331.

McGoldrick, L. F. 1970 On Wilton's ripples: a special case of resonant interactions. *J. Fluid Mech.* **42**, 193–200.

Miles, J. W. 1962 On the generation of surface waves by shear flows. Part 4. *J. Fluid Mech.* **13**, 433–448.

Miles, J. W. 1976 On internal resonance of two damped oscillators. *Stud. Appl. Maths* **55**, 351–359.

Morland, L. C. 1994 Resonant triads of capillary–gravity waves in the presence of a current. *Phys. Fluids* **6**, 588–594.

Nayfeh, A. H. 1973 Second-harmonic resonance in the interaction of an air stream with capillary-gravity waves. *J. Fluid Mech.* **59**, 803–816.

Pierson, W. J. & Fife, P. 1961 Some nonlinear properties of long-crested periodic waves with lengths near 2.44 centimeters. *J. Geophys. Res.* **66**, 163–179.

Ramamonjiarisoa, A., Baldy, S. & Choi, I. 1978 Laboratory studies on wind-wave generation, amplification and evolution. In *Turbulent Fluxes through the Sea Surface, Wave Dynamics, and Prediction* (ed. A. Favre & K. Hasselmann), pp. 403–420. Plenum.

Shemdin, O. H 1972 Wind-generated current and phase speed of wind waves. *J. Phys. Oceanogr.* **2**, 411–419.

Simmons, W. F. 1969 A variational method for weak resonant wave interactions. *Proc. R. Soc. Lond.* A **309**, 551–575.

Strizhkin, I. I. & Raletnev, V. I. 1986 Experimental studies of three- and four-wave resonant interactions of surface sea waves. *Izv. Atmos. Ocean. Phys.* **22**(4), 311–314.

Trulsen, K. 1995 The influence of currents, long waves and wind on gravity–capillary waves. PhD thesis, Massachusetts Institute of Technology.

Trulsen, K. & Mei, C. C. 1995 Modulation of three resonating gravity-capillary waves by a long gravity wave. *J. Fluid Mech.* **290**, 345–376.

Valenzuela, G. R. 1976 The growth of gravity-capillary waves in a coupled shear flow. *J. Fluid Mech.* **76**, 229–250.

Vyshkind, S. Y. & Rabinovich, M. I. 1976 The phase stochastization mechanism and the structure of wave turbulence in dissipative media. *Sov. Phys. JETP* **44**, 292–299.

Wersinger, J.-M., Finn, J. M. & Ott, E. 1980*a* Bifurcations and strange behavior in instability saturation by nonlinear mode coupling. *Phys. Rev. Lett.* **44**, 453–456.

Wersinger, J.-M., Finn, J. M. & Ott, E. 1980*b* Bifurcation and "strange" behavior in instability saturation by nonlinear three-wave mode coupling. *Phys. Fluids* **23**, 1142–1154.

Wilton, J. R. 1915 On ripples. *Phil. Mag.* **29**, 688–700.